Chemical Papers
https://doi.org/10.1007/s11696-024-03444-z

ORIGINAL PAPER

Ultra-small carbon quantum dots via *Hibiscus Sabdariffa* for pyridoxine sensing applications

J. D. Amador-Martínez[1] · P. G. Mani-Gonzalez[2] · G. Calderón-Ayala[3] · A. Navarro-Badilla[4] · J. E. Leal-Pérez[5] · C. Leyva-Porras[6] · N. S. Flores-López[3] · R. Britto Hurtado[1] · M. Flores-Acosta[1] · M. Cortez-Valadez[7]

Received: 8 August 2023 / Accepted: 9 March 2024

Abstract

This study proposes an alternative for producing carbon quantum dots through green synthesis using *Hibiscus sabdariffa* as a carbon source. The synthesis methodology incorporates mesoporous zeolite 4A as a refractory material during thermal treatment and as a sieve for particle size selection. Transmission electron microscopy (TEM) analysis revealed a narrow size distribution of approximately 1.2 nm, aligning with the α-cage diameter of zeolite 4A. Additionally, the CQDs were evaluated as surface-enhanced Raman spectroscopy substrates on a pyridoxine molecule ($C_8H_{11}NO_3$), which showed an enhancement of the pyridinic ring breathing mode at approximately 1000 cm^{-1}. Furthermore, employing density functional theory (DFT), several carbon structures were theoretically used to represent the CQD–pyridoxine interaction. Based on the molecular descriptor behavior, the charge transfer effects between both systems were studied to determine the elements responsible for the SERS effect associated with the chemical enhancement mechanism. This comprehensive approach provides insight into the structural and optical properties of the synthesized CQDs, with significant implications for their potential application in different areas, particularly in SERS.

Keywords Carbon quantum dots · Green synthesis · SERS effect · Chemical enhancement mechanism

Introduction

Since their discovery, CQDs (carbon quantum dots) have attracted the interest of the scientific community, leading to novel applications and promising methods for obtaining them (El-Malla et al. 2022; Kalashgrani et al. 2022). Some important applications of CQDs include photoluminescence detection, bioimaging, biosensors, photocatalysis, energy stage accumulation, biomedicine, and theranostic treatments (El-Malla et al. 2022; Feng and Qian 2018; Hoang et al. 2019; Kalashgrani et al. 2022; Luo et al. 2013; Wang et al. 2017; Yang et al. 2014). CQDs have been used for mercury detection, cellule imaging, contaminant separation, and solar cell sensors (Guo et al. 2017; Ramar et al. 2018; Selvaraju et al. 2022; Tadesse et al. 2020, 2018).

Several top-down and bottom-up methods for obtaining CQDs are currently available in the literature, including laser ablation, thermal decomposition, controlled chemical oxidation, hydrolysis of organic molecules, hydrothermal synthesis, and pyrolysis of polymer precursors (Cui et al. 2020; Li et al. 2022; Sahadev and Anappara 2020; Wang and Hu 2014; Wu et al. 2017; Zulfajri et al. 2021).

✉ M. Cortez-Valadez
manuelcortez@live.com

1 Departamento de Investigación en Física, Universidad de Sonora, Apdo. Postal 5-88, 83190 Hermosillo, Sonora, México

2 Department of Physics and Mathematics, Institute of Engineering and Technology, Autonomous University of Ciudad Juárez, 32310 Cd. Juárez, México

3 Universidad Estatal de Sonora, Rosales No. 189 Col. Centro, 83100 Hermosillo, México

4 Departamento de Física, Universidad de Sonora, 83000 Hermosillo, Sonora, México

5 Universidad Autónoma de Sinaloa, Fuente de Poseidón y Prol. Ángel Flores S/N., 81223 Los Mochis, Sinaloa, México

6 Centro de Investigación en Materiales Avanzados S.C. (CIMAV), Chihuahua 31136, México

7 CONAHCYT-Departamento de Investigación en Física, Universidad de Sonora, Apdo. Postal 5-88, 83190 Hermosillo, Sonora, México

Published online: 15 April 2024

Additionally, an efficient, stable, and low-cost synthesis method for this system uses natural organic compounds as carbon sources. Soya Milk was used to obtain CQDs with photoluminescence properties and electrocatalytic applications (Malavika et al. 2022). After this finding, a vast exploration by the related scientific community was carried out, achieving representative results in the synthesis of CQDs. These plant extracts, leaves, roots, fungi, etc., are used to obtain CQDs by hydrothermal processes (Bano et al. 2018; Baweja and Jeet 2019; Zhu et al. 2021). These representative results are associated with the particle size control and emission band dependence of the configuration parameters during the synthesis process (Das et al. 2018).

In this context, the biosynthesis of CQDs has undergone notable advances, focusing on the use of natural sources such as *Azadirachta indica, Allium cepa, Echinops persicus, and Citrus paradisi*, among others (Ghosh Dastidar et al. 2021; Nasseri et al. 2020; Xiao et al. 2018; Yadav et al. 2019). This route stands out for its sustainable approach but also diversifies the chemical composition and properties of the resulting CQDs. In this process, molecules or compounds with a high carbon content are used as carbon precursors, allowing stable CQDs to be obtained while avoiding toxic compounds in so-called green synthesis. Notably, the usefulness of plant extracts as carbon sources for synthesizing CQDs, providing an environmentally friendly alternative, has been highlighted. A notable example is the work of Hoan et al., who used an extract of *Citrus lemon* in hydrothermal processes to obtain CQDs with reduced sizes, even reaching 20 nm (Hoan et al. 2019). Other reports have also explored the synthesis of CQDs using plant extracts such as *Calotropis gigantea*, employing microwave radiation to obtain CQDs with narrow particle size distributions (Sharma et al. 2022). In addition to advances in the synthesis process, the primary application of CQDs continues to be their development as fluorescent biosensors or bioimaging agents (Ashok Kumar et al. 2023; Caglayan et al. 2022; Janus et al. 2020). These advances have significantly promoted molecular sensing and cellular visualization, taking advantage of the specific properties of CQDs, such as their fluorescence and biocompatibility. In contrast, using CQDs as SERS sensors (nonconjugated or nonfunctionalized) are in an initial research phase, with few results reported to date. The detection of melamine/pristine, pyridine, and avapritinib, which serve as promising evidence of the ability of CQDs to identify compounds of interest through the SERS technique, is particularly promising (Alsalme et al. 2021; Kong et al. 2012; Sharma et al. 2019). The limited number of existing results highlights the opportunity for more detailed research in this area, potentially opening up new possibilities for designing susceptible and specific sensors based on CQDs. In contrast, the functionalization or conjugation of CQDs with various molecular and nanostructured systems for SERS sensing has been widely studied and continues to be actively addressed. However, this topic was not considered in the present study.

On the other hand, CQDs are distinctive because of their inherent negative surface charge (Wang et al. 2017). Thus, the interactions of CQDs with specific molecules can be susceptible to electronic transitions. The CT (charge transfer) mechanism is related to the surface-enhanced Raman spectroscopy (SERS) effect. The electromagnetic enhanced mechanism (EEM) and chemical enhanced mechanism (CEM) theories are associated with this effect. The EEM is associated with metallic nanostructured systems and originated from surface plasmon resonance, and CEMs are associated with nonmetallic systems. The EEM and CEM are responsible for Raman mode intensifications on the order of 10^{13} and 10^{3}, respectively (Wang et al. 2017). The CEM mechanism considers electron transfer between the CQDs and the molecule, leading to Raman transitions.

This study presents an alternative for obtaining CQDs through green synthesis in combination with zeolite as a sieve. Additionally, this study considered CEM for analyzing the charge transfer between pyridoxine molecules and carbon structures, thus exploring its influence on SERS behavior.

Materials and methods

Experimental details

The *Hibiscus sabdariffa* (Jamaica flower) plant was used as a carbon source. Subsequently, 20 g of *Hibiscus sabdariffa* was added, and 50 ml of deionized water was added to obtain the extract. The infusion was kept under magnetic stirring at 70 °C for 1 h, after which the solution was filtered to remove microscopic particles. The resulting extract was mixed with 2 g of synthetic zeolite A4 and magnetically stirred at 155 °C for 1 h. The extract on the zeolite matrix was subjected to heat treatment at 200 °C for 2 h in an electric oven. The obtained calcined samples were finely pulverized in an agate mortar, and 0.25 g of each sample was extracted and sonicated with 6 ml of distilled water for 1 min. Finally, the samples were poured into test tubes and subjected to 11,000 revolutions per minute for 5 min to remove the residues. This solution contains colloidal CQDs.

Theoretical calculations

Complementarily, theoretical analysis is considered to predict the energy levels of the frontier molecular orbitals of the pyridoxine and carbon structures representing the CQDs. On this basis, we determined molecular descriptors such as the reorganization energy and the charge transfer integral, which depend on the electronic

behavior of the system and provide insight into the SERS effect. Therefore, the structures C_6H_6, $C_{14}H_{10}$, $C_{20}H_{12}$ and $C_{22}H_{12}$ interacted with the pyridoxine molecule ($C_8H_{11}NO_3$) according to density functional theory (DFT) at B3LYP (Becke, three-parameter, Lee–Yang–Parr) in combination with the 6-31G basis set. In all cases, the systems were optimized to find the minimum local energy.

TEM images were obtained using a JEOL JEM 2200FS + CS transmission electron microscope. Absorbance spectra were obtained using a UV/VIS VeLab 5100UV in the 200–800 nm region. A LabRAM HR Evolution instrument with a 785 nm laser wavelength was used for Raman spectroscopy and to determine the effect of SERS on pyridoxine.

Results and discussion

TEM characterization allowed analysis of the structural and morphological properties of the CQDs, as shown in Fig. 1a. These are distributed without agglomerations. A uniform distribution improves the stability and functionality of CQDs for several applications (Wang et al 2017). The size of the CQDs is between 0.6 and 1.6 nm, as identified in the particle size histogram in Fig. 1b. These values reveal the narrow size distribution of the CQDs in the analyzed sample.

In addition, we observe that the highest percentage of particles are 1.2 nm in size and have a dot-like behavior. This implies that the CQDs have a well-defined structure and behave as individual entities rather than forming aggregates or larger arrangements. We assume that the

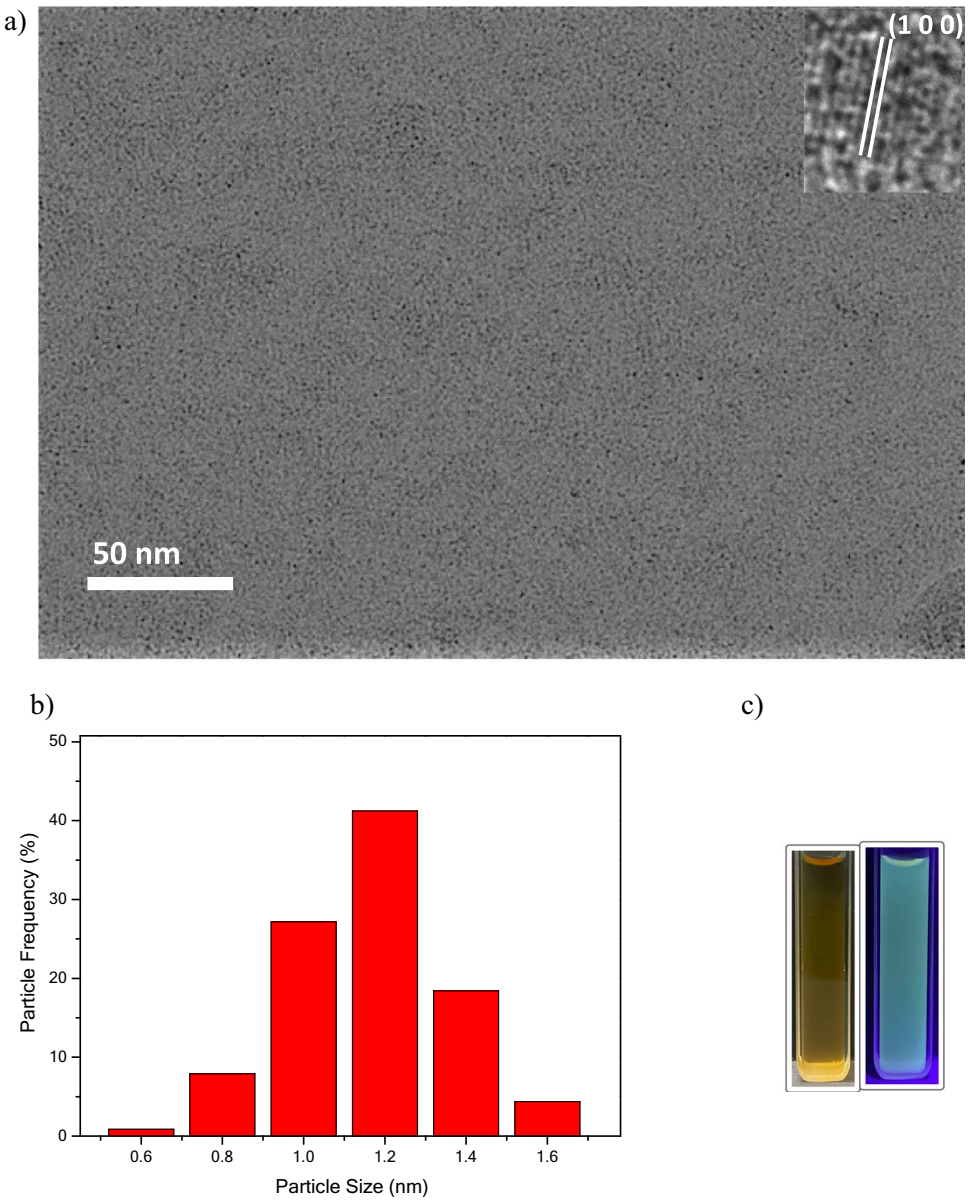

Fig. 1 **a** TEM image of CQDs from *Hibiscus sabdariffa* (inset interplanar distance of 2.14 Å associated with (1 0 0) Miller indices), **b** particle size histogram, and **c** photoluminescence effect in the CQDs

zeolite 4A channels play an important role in delimiting the size of the CQDs by hosting molecular amounts of the extract components before the carbonization process. The predominant size obtained may be relevant to the properties and applications of CQDs in biosensing (Wang et al. 2017). Complementarily, UV light (340 nm) was incident on the CQDs, achieving emissions in the blue region (Fig. 1c) due to electronic transitions of electrons that are relaxed at lower energy levels, generating visible light. This confirmed that the CQDs were in the colloidal solution.

The UV−Vis spectrum of the *Hibiscus sabdariffa* extract is shown in Fig. 2a. The $\pi \rightarrow \pi^*$ electronic transition occurs when an electron is excited from a π orbital (double bond) to a π^* (anti-bonding) orbital. This transition is associated with the C=C bonds in the CQDs obtained from the Hibiscus sabdariffa extract. This band localized at approximately 200 nm is shown in Fig. 2b. The samples were analyzed under different thermal treatment conditions in an oven. Carbonization occurred due to the disappearance of the bands associated with the extracted components in the UV−Vis spectrum. In this case, heat treatment caused the extract components to undergo this transformation, likely resulting in chemical composition and property changes. This process leads to the thermal decomposition of some organic molecules, which breakdown into simpler compounds, some of which are released as gas and leave a residue of carbonaceous material. Through this process, some bonds present in the components of the extract are broken, resulting in the disappearance of the bands identified in the UV−Vis spectrum. (Supplemental information Figure S1). FTIR analysis was carried out to determine the functional groups in the CQDs that could impart specific stability (Supplemental information Figure S2).

The Raman spectra of the CQDs obtained with *Hibiscus sabdariffa* flower extract at different temperatures after interacting with pyridoxine (Pd) are shown in Fig. 3. For the vibrational mode located at approximately 1000 cm^{-1}, there is an increase in the Raman intensity associated with the pyridoxine breathing mode, which is susceptible to the

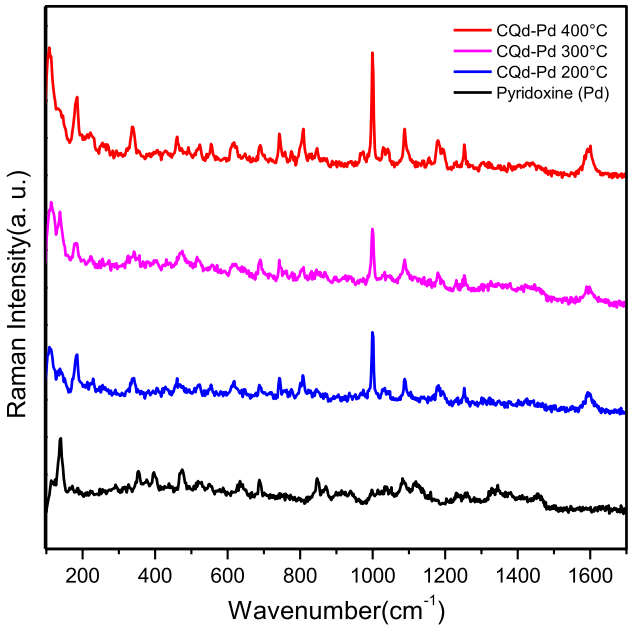

Fig. 3 Raman spectra of pyridoxine (black line) and CQD-pyridoxine interactions obtained from *Hibiscus sabdariffa* flowers at different temperatures during synthesis

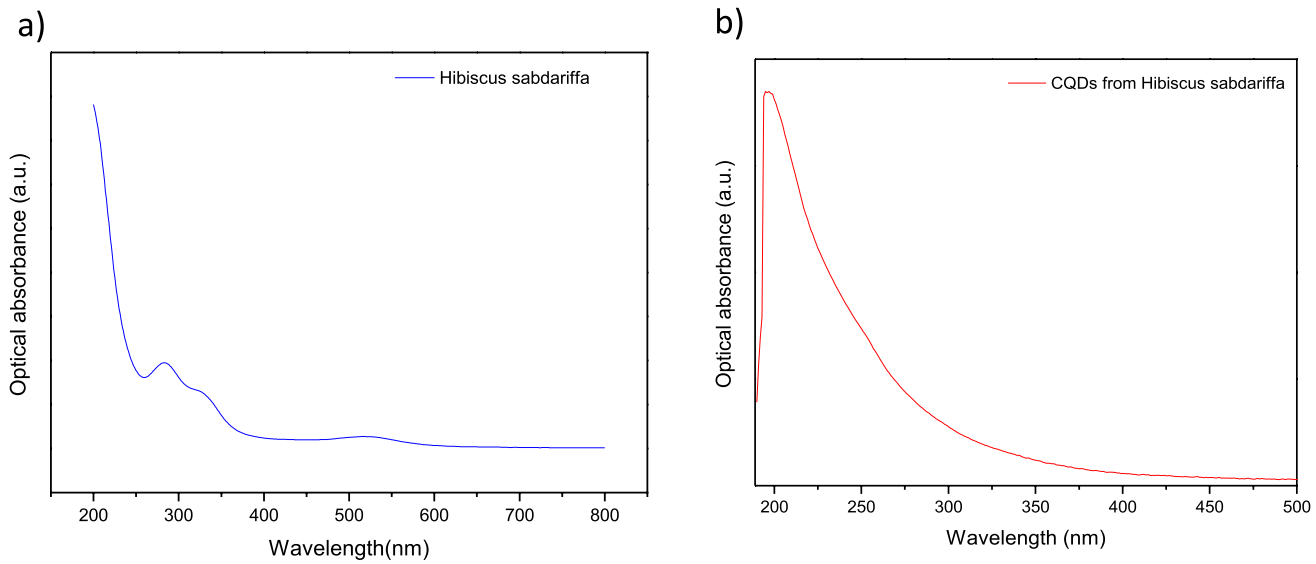

Fig. 2 UV−Vis spectra of the **a** *Hibiscus sabdariffa* extract and **b** CQDs

effects of SERS (electromagnetic and chemical enhancement mechanisms). This mode can be shifted between 600 and 1100 cm^{-1} depending on the type of interacting system (Hoang et al. 2019).

Pyridoxine is a molecule with higher structural complexity than pyridine and presents vibrational modes with similar relative intensities (mostly skeletal modes) between 200 and 2000 cm^{-1}. Only the radial breathing mode (RBM) associated with the pyridine ring mentioned above stands out. In other interacting systems with CQDs, a band associated with bending vibrations (O–H) located at 1590 cm^{-1} has been identified. The highest RBM intensity is located in the spectrum obtained with thermal treatment at 400 °C. This is associated with the UV−Vis results, where the absorption bands decrease due to the temperature. This approach can improve interactions by significantly reducing contaminants, allowing a more integrated Raman spectrum. Regarding the factors that can promote SERS enhancement, the morphology, aggregation state, and nature of the CQDs are critical parameters for achieving an adequate homogeneous dispersion of the specific regions on the CQD (hot spot) surface, which can considerably increase the SERS effect.

Additionally, we present a table comparing the analytical performance of our pyridoxine detection SERS substrate with that of recently reported SERS substrates (Table 1).

The charge transfer degree (ρ) is a quantitative measure of the relative charge transfer contribution to the intensity of the SERS effect, defined by Lombardi and Birke by the following equation (Lombardi and Birke 2009):

$$\rho = \frac{R}{1+R} \tag{1}$$

The magnitude of ρ in the SERS effect indicates the predominant type of contribution to the enhancement of the amplified Raman band. A value close to 1 indicates a dominance of charge transfer, a value close to 0 indicates a contribution mainly due to chemical bonding factors, and a value of approximately 0.5 implies a similar influence of both types of contributions. To obtain the ρ for the Raman spectra in Fig. 3, two intensities of two vibrational modes of each spectrum are selected, symmetric (I_S) and antisymmetric (I_{AS}), to determine the value of R (given by the ratio between the intensity of a symmetric bending mode and an asymmetric stretching mode of the analyte) and thereby determine the ρ. Furthermore, ρ is closer to 1 for each spectrum. This is associated with the predominant charge transfer in the SERS effect, as shown in Table 2. The ρ is higher for the case where the CQDs were exposed to 400 °C (Fig. 3, red line).

In the DFT framework, we consider representative models of CQDs as carbon surface systems, which provide us with details of their optical and structural behavior and information on their molecular orbitals and charge transfer interactions. For this purpose, we assumed specific systems, such as C_6H_6 (1R), $C_{14}H_{10}$ (2R), $C_{20}H_{12}$ (5R) and $C_{22}H_{12}$ (6R), as representative of the CQD surface, as shown in Fig. 4a, which interacted with pyridoxine (Fig. 4b). In these systems, CEM contributions are generally related to the energy levels of the HOMO–LUMO (highest occupied molecular orbital–lowest unoccupied molecular orbital) molecular orbitals and the influence of electron transfer. The CEM mechanism is responsible for the SERS effect in semiconductor systems such as CQDs. This mechanism has achieved enhancement factors on the order of up to 10^3 (Hoang et al. 2019).

Additionally, an important parameter is the fraction of electrons transferred (ΔN), which is related to the electronegativity χ and global hardness η according to the Pearson method:

$$\Delta N = \frac{\chi_{\text{S. de Carbono}} - \chi_{\text{Molecula}}}{2\left(\eta_{\text{S. de Carbono}} + \eta_{\text{Molecula}}\right)} \tag{2}$$

where

Table 2 Charge transfer degree (ρ)

Interacting system	I_S	I_{AS}	R	ρ
CQD-Pd 200 °C	226.1	105.2	2.1	0.68
CQD-Pd 300 °C	220.8	136.7	1.6	0.62
CQD-Pd 400 °C	341.8	120.9	2.8	0.74

Table 1 Comparative table of the analytical performance of pyridoxine SERS sensing

Substrate	Enhancement mechanism	Enhancement factor	References
Au–Sn	EEM and CEM	~ 10^2	Chu et al. (2009)
Ag	EEM	–	Cinta et al. (1999)
Ag	CEM	~ 10^1	Horta-Piñeres et al. (2022)
Adenine	CEM	< 10^1	Roye et al. (2019)
Au	EEM	~ 10^5	Ibáñez et a. (2020)
CQDs	CEM	~ 10^2	This work

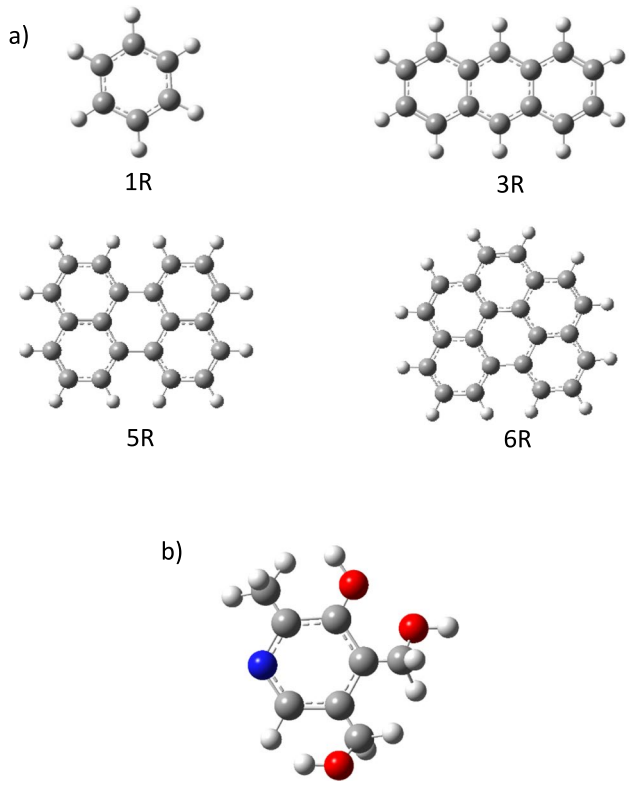

Fig. 4 **a** Representation of the CQD surface: C_6H_6 (1R), $C_{14}H_{10}$ (2R), $C_{20}H_{12}$ (5R) and $C_{22}H_{12}$ (6R) and **b** Pyridoxine molecule

$$\chi = \frac{-\text{HOMO} - \text{LUMO}}{2}$$
$$y\eta = \frac{-\text{HOMO} + \text{LUMO}}{2} \quad (3)$$

The fraction of electrons transferred will consider the difference in electronegativity since it occurs from a molecule with a lower electronegativity to a molecule with a higher electronegativity. Considering this, a fraction of electron transfer from the CQD to the molecule will occur if $\Delta N < 0$, and for the opposite case, where $\Delta N > 0$ electron transfer from the molecule to the CQD.

Based on the obtained values for the HOMO–LUMO energy levels, global hardness, and electronegativity, the fraction of electrons transferred and the electron transfer pathway are shown in Table 3. In all cases, we observe that the fraction of electrons transferred is negative, so the electron transfer pathway is from the CQD to the Pd molecule.

Additionally, visualization of the electron transfer pathway was performed for representative CQD systems: C_6H_6 (1R), $C_{14}H_{10}$ (2R), $C_{20}H_{12}$ (5R), $C_{22}H_{12}$ (6R) and Pd. These results agree with the fraction of electrons transferred, so the electron transfer pathway occurs from the carbon systems to pyridoxine, as shown in Table 2.

Table 3 Fraction of electrons transferred and electron transfer pathway after 1R-Pd, 3R-Pd, 5R-Pd and 6R-Pd interacting systems

Interacting system	Fraction of electrons transferred (e^-)	Electron transfer pathway
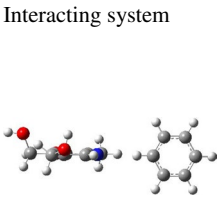	−0.055	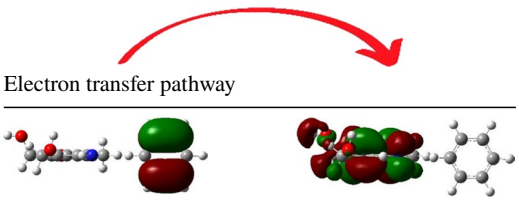
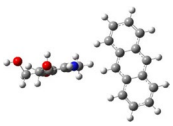	−0.067	
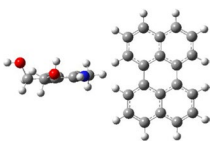	−0.014	
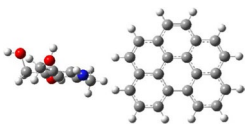	−0.012	

Conclusions

Considering the conditions and experimental parameters selected to obtain CQDs using *Hibiscus sabdariffa* extract as a carbon source, we determined that these systems are well distributed without agglomeration and present an ultra-small particle size centered at 1.2 nm. These results confirmed that synthetic zeolite A4 can act as a sieve, delimiting the size of the CQDs. The UV/Vis spectra showed an absorption band attributed to carbon systems, close to 200 nm, associated with $\pi \rightarrow \pi^*$ electronic transitions. This transition was attributed to the C=C bonds in the CQDs obtained from the *Hibiscus sabdariffa* extract.

Due to charge transfer effects, the interaction between pyridoxine as a probe molecule and the CQD solutions promoted the enhancement of the experimental intensity of the pyridoxine-specific Raman modes through the CEM. Complementarily, molecular descriptors in the DFT framework allowed us to determine the presence of electron transfer between carbon structures and pyridoxine. In addition, we aimed to determine clues about the prediction and electron transfer pathway between the interacting systems.

The ultra-small size and narrow distribution of the CQDs obtained by this synthesis method render them viable candidates for selectively interacting with biomolecules of interest and generating detectable optical signals for SERS sensing. This approach may enable the detection of several biomolecules in theranostics applications, environmental monitoring, and biological studies.

Supplementary Information The online version contains supplementary material available at https://doi.org/10.1007/s11696-024-03444-z.

Acknowledgements The computational resources for this investigation were provided by UNISON/ACARUS. The author M. Cortez-Valadez appreciates support from the "Investigadores por México" program.

Author contributions JDAM was contributed to data curation, methodology, formal analysis, investigation, writing—original draft. PGM-G was contributed to conceptualization and validation. GC-A was contributed to visualization, connectivity, and supercomputer setup. AN-B was contributed to optical characterization and validation. JEL-P was contributed to Raman spectroscopy characterization and validation. CL-P was contributed to TEM analysis. RBH was contributed to vibrational spectroscopy characterization and validation. NSF-L was contributed to vibrational spectroscopy and visualization. MF-A was contributed to project administration, funding acquisition, visualization. MC-V was contributed to resources, funding acquisition, supervision, validation, visualization, review and editing.

Funding This work was supported by Basic Science Project A1-S-46242 of the CONAHCYT.

Data availability The data that support the findings of this study are available from the corresponding author upon reasonable request.

Declarations

Conflict of interest The authors have no conflicts to disclose.

References

Alsalme A, Pooventhiran T, Al-Zaqri N, Rao DJ, Thomas R (2021) Structural, physico-chemical landscapes, ground state and excited state properties in different solvent atmosphere of Avapritinib and its ultrasensitive detection using SERS/GERS on self-assembly formation with graphene quantum dots. J Mol Liq 322:114555

Ashok Kumar S, Dheeraj Kumar M, Saikia M, Renuga Devi N, Subramania A (2023) A review on plant derived carbon quantum dots for bio-imaging. Mater Adv 4:3951–3966

Bano D, Kumar V, Singh VK, Hasan SH (2018) Green synthesis of fluorescent carbon quantum dots for the detection of mercury(II) and glutathione. New J Chem 42:5814–5821

Baweja H, Jeet K (2019) Economical and green synthesis of graphene and carbon quantum dots from agricultural waste. Mater Res Express 6:0850g8

Caglayan MO, Mindivan F, Şahin S (2022) Sensor and bioimaging studies based on carbon quantum dots: the green chemistry approach. Crit Rev Anal Chem 52:814–847

Chu Y, Chen S, Zheng J, Li Z (2009) Elimination of oxidation and decomposition by SnCl2 in the SERS study of pyridoxine on a roughened Au electrode. J Raman Spectrosc 40(2):229–233

Cinta S, Morari C, Vogel E, Maniu D, Aluas M, Iliescu T, Cozar O, Kiefer W (1999) Vibrational studies of B6 vitamin. Vib Spectrosc 19(2):329–334

Cui L, Ren X, Wang J, Sun M (2020) Synthesis of homogeneous carbon quantum dots by ultrafast dual-beam pulsed laser ablation for bioimaging. Mater Today Nano 12:100091

Das R, Bandyopadhyay R, Pramanik P (2018) Carbon quantum dots from natural resource: a review. Mater Today Chem 8:96–109

El-Malla SF, Elshenawy EA, Hammad SF, Mansour FR (2022) Rapid microwave synthesis of N, S-doped carbon quantum dots as a novel turn off-on sensor for label-free determination of copper and etidronate disodium. Anal Chim Acta 1197:339491

Feng H, Qian Z (2018) Functional carbon quantum dots: a versatile platform for Chemosensing and Biosensing. Chem Rec 18:491–505

Ghosh Dastidar D, Mukherjee P, Ghosh D, Banerjee D (2021) Carbon quantum dots prepared from onion extract as fluorescence turn-on probes for selective estimation of Zn2+ in blood plasma. Colloids Surfaces A Physicochem Eng Asp 611:125781

Guo X, Zhang H, Sun H, Tade MO, Wang S (2017) Green synthesis of carbon quantum dots for sensitized solar cells. ChemPhotoChem 1:116–119

Hoan BT, Tam PD, Pham VH (2019) Green synthesis of highly luminescent carbon quantum dots from lemon juice. J Nanotechnol 2019

Hoang VC, Dave K, Gomes VG (2019) Carbon quantum dot-based composites for energy storage and electrocatalysis: mechanism, applications and future prospects. Nano Energy 66:104093

Horta-Piñeres S, Cortez-Valadez M, Avila DA, Leal-Perez JE, Hurtado-Macías A, Flores-Acosta M, Torres CO (2022) Green synthesis of silver nanoparticles via Bougainvillea Spectabilis (leaves and stem) for pyridoxine SERS sensing. Appl Phys A 128(12):1090

Ibáñez D, Pérez-Junquera A, González-García MB, Hernández-Santos D, Fanjul-Bolado P (2020) Spectroelectrochemical elucidation of B vitamins present in multivitamin complexes by EC-SERS. Talanta 206:120190

Janus Ł, Radwan-Pragłowska J, Piatkowski M, Bogdał D (2020) Facile synthesis of surface-modified carbon quantum dots (CQDs) for biosensing and bioimaging. Materials 13:3313

Kalashgrani MY, Nejad FF, Rahmanian V (2022) Carbon quantum dots platforms: as nano therapeutic for biomedical applications. Adv Appl Nanobio-Technol 3:38–42

Kong X, Chen Q, Li R, Cheng K, Yan N, Chen J, Zhou Y (2012) Theoretical investigation on SERS of pyridine adsorbed on Cn clusters induced by charge transfer: a hint that SERS could be applied on many materials. ChemPhysChem 13:1449–1453

Li X, Liu X, Su Y, Jiang T, Li D, Ma X (2022) Green synthesis of carbon quantum dots from wasted enzymatic hydrolysis lignin catalyzed by organic acids for UV shielding and antioxidant fluorescent flexible film. Ind Crops Prod 188:115568

Lombardi JR, Birke RL (2009) A unified view of surface-enhanced Raman scattering. Acc Chem Res 42:734–742

Luo PG, Sahu S, Yang ST, Sonkar SK, Wang J, Wang H, Lecroy GE, Cao L, Sun YP (2013) Carbon "quantum" dots for optical bioimaging. J Mater Chem B 1:2116–2127

Malavika JP, Shobana C, Sundarraj S, Ganeshbabu M, Kumar P, Selvan RK (2022) Green synthesis of multifunctional carbon quantum dots: an approach in cancer theranostics. Biomater Adv 136:212756

Nasseri MA, Keshtkar H, Kazemnejadi M, Allahresani A (2020) Phytochemical properties and antioxidant activity of Echinops persicus plant extract: green synthesis of carbon quantum dots from the plant extract. SN Appl Sci 2:1–12

Ramar V, Moothattu S, Balasubramanian K (2018) Metal free, sunlight and white light based photocatalysis using carbon quantum dots from Citrus grandis: a green way to remove pollution. Sol Energy 169:120–127

Roye Y, Udeochu U, Ukaegbu M, Onuegbu J (2019) Spectroelectrochemical investigation of the interaction of adenine with pyridoxine at physiological pH. J Spectrosc 2019:6979547

Sahadev N, Anappara AA (2020) Photo-to-thermal conversion: effective utilization of futile solid-state carbon quantum dots (CQDs) for energy harvesting applications. New J Chem 44:10662–10670

Selvaraju N, Selvaraj S, Singhal N, Mohan V, Sivalingam Y, Rajaram K, Venugopal G (2022) Electron transfer behaviour of green synthesized carbon quantum dot sensor towards VOC and heavy metal ion sensing. Mater Sci Eng B 282:115792

Sharma V, Kagdada HL, Singh DK, Jha PK (2019) Trapping melamine with pristine and functionalized graphene quantum dots: DFT and SERS studies. Springer Proc Phys 236:441–451

Sharma N, Sharma I, Bera MK (2022) Microwave-assisted green synthesis of carbon quantum dots derived from Calotropis Gigantea as a fluorescent probe for Bioimaging. J Fluoresc 32:1039–1049

Tadesse A, Rama Devi D, Hagos M, Battu G, Basavaiah K (2018) Facile green synthesis of fluorescent carbon quantum dots from citrus lemon juice for live cell imaging. Asian J Nanosci Mater 1:36–46

Tadesse A, Hagos M, Ramadevi D, Basavaiah K, Belachew N (2020) Fluorescent-nitrogen-doped carbon quantum dots derived from citrus lemon juice: green synthesis, Mercury(II) ion sensing, and live cell imaging. ACS Omega 5:3889–3898

Wang Y, Hu A (2014) Carbon quantum dots: synthesis, properties and applications. J Mater Chem C 2:6921–6939

Wang R, Lu KQ, Tang ZR, Xu YJ (2017) Recent progress in carbon quantum dots: synthesis, properties and applications in photocatalysis. J Mater Chem A 5:3717–3734

Wu P, Li W, Wu Q, Liu Y, Liu S (2017) Hydrothermal synthesis of nitrogen-doped carbon quantum dots from microcrystalline cellulose for the detection of Fe 3+ ions in an acidic environment. RSC Adv 7:44144–44153

Xiao P, Ke Y, Lu J, Huang Z, Zhu X, Wei B, Huang L (2018) Photoluminescence immunoassay based on grapefruit peel-extracted carbon quantum dots encapsulated into silica nanospheres for p53 protein. Biochem Eng J 139:109–116

Yadav PK, Singh VK, Chandra S, Bano D, Kumar V, Talat M, Hasan SH (2019) Green synthesis of fluorescent carbon quantum dots from Azadirachta Indica leaves and their peroxidase-mimetic activity for the detection of H_2O_2 and ascorbic acid in common fresh fruits. ACS Biomater Sci Eng 5:623–632

Yang S, Sun J, Li X, Zhou W, Wang Z, He P, Ding G, Xie X, Kang Z, Jiang M (2014) Large-scale fabrication of heavy doped carbon quantum dots with tunable-photoluminescence and sensitive fluorescence detection. J Mater Chem A 2:8660–8667

Zhu L, Shen D, Wang Q, Luo KH (2021) Green synthesis of tunable fluorescent carbon quantum dots from lignin and their application in anti-counterfeit printing. ACS Appl Mater Interfaces 13:56465–56475

Zulfajri M, Sudewi S, Ismulyati S, Rasool A, Adlim M, Huang GG (2021) Carbon dot/polymer composites with various precursors and their sensing applications: a review. Coatings 11:1100